Continuous acid-catalyzed esterification using a 3D printed rotor–stator hydrodynamic cavitation reactor reduces free fatty acid content in mixed crude palm oil

Ye Min Oo, Gumpon Prateepchaikul, Krit Somnuk[*]

Department of Mechanical Engineering, Faculty of Engineering, Prince of Songkla University, Hat Yai, Songkhla 90110, Thailand

ARTICLE INFO

ABSTRACT

Free fatty acid (FFA) content in FFA-rich mixed crude palm oil (MCPO) was reduced through a continuous esterification process. The reaction conditions were optimized, the yield purified esterified oil was determined, and the average total electricity consumption of the entire process was evaluated. The key component of this study was the cost-effective, 3D-printed rotor that was installed in a continuous rotor–stator hydrodynamic reactor. The surface of the rotor was designed with spherical holes where the center-to-center distance between them was fixed. Response surface methodology (RSM) using central composite design (CCD) was employed to analyze the design of experiments (DOE) and optimize FFA-content reduction. The optimized conditions were 17.7 vol% methanol, 2.9 vol% sulfuric acid, a 3000 rpm rotor speed, and surface holes measuring 4 mm in diameter and 6 mm in depth. The experimental results showed that the FFA content in MCPO was reduced from 11.456 to 1.028 wt% upon esterification under these optimal conditions. The maximum yield of esterified oil from the phase separation step was 96.07 vol%, and that of the purified esterified oil was 91.27 vol%. The average total energy consumed by this hydrodynamic cavitation reactor to produce this esterified oil was 0.0264 kW h/L. This 3D printed rotor–stator reactor is a promising, novel reactor technology for producing biodiesel from FFA-rich oils.

1. Introduction

Biodiesel is a highly effective alternative fuel used in transportation sectors worldwide, such as those in the United States, Canada, Australia, Japan, China, and other Asian countries [1,2]. Global biodiesel consumption rapidly increased from 19.5 to 43.5 billion liters between 2010 and 2019 [1]. The United States, Brazil, and Argentina produce the largest amounts of biodiesel; specifically, 7.2, 4.5, and 4 billion liters, respectively [1]. Indonesia and Thailand are the leaders in biodiesel production among the Asian countries and are the 4th and 5th largest oil producers worldwide, respectively [1,3,4]. In 2019, approximately 85% of global palm oil was produced by Indonesia and Malaysia [5,6]. During the same year, Thailand produced an average of 1.843 billion liters of biodiesel from approximately 1.398 million tons of crude palm oil (CPO) [7]. Diesel B7 (7% biodiesel with 93% diesel) is currently the standard diesel used in Thailand. At present, the Thailand Ministry of Energy has designated diesel B10 as the standard diesel to be used in Thailand beginning on October 1, 2020 [8]. Moreover, the ministry has

encouraged diesel B20 to be used by heavy trucks and buses [9]. Therefore, mixing biodiesel with diesel is becoming increasingly necessary. Furthermore, utilizing biodiesel will reduce air pollution; specifically, the amount of aggravating smog in the atmosphere. Particulate matter ($PM_{2.5}$) makes up 70% of gas emission, is harmful to the body, and causes respiratory diseases [10]. Therefore, the Thailand Ministry of Energy has partly promoted diesel B10 and B20 to decrease the concentration of $PM_{2.5}$ air pollutants [11]. Generally, biodiesel can be produced from both edible oils (sunflower, soybean, and coconut) and non-edible oils (microalgae, jatropha, Karanja, neem, mahua, rubber seed, and silk-cotton). However, there are some problems inhibiting biodiesel production from edible oils, such as increasing costs for the edible-oil market and biodiesel production [12]. This is because the feedstock cost is considered when producing biodiesel. CPO is one of the most productive sources of vegetable oil, where palm oil plantations 1 ha in size can produce up to 3.5 tons of oil. The second most productive crop is canola oil, which can be produced in quantities of 0.8 tons per hectare. Therefore, it is evident that the production capacity rate of palm

---

oil per unit area is higher than that of other vegetable oil crops [13]. Furthermore, CPO is considered one of the richest sources for producing biodiesel and is one of the most rapidly expanding, cheap, tropical plant species. In Malaysia, palm oil plantations are one of the largest sectors that provide income and employment for many rural communities [14,15]. However, CPO is rich in free fatty acids (FFAs), which can react with alkaline catalysts and produce soap via saponification [16,17]. Therefore, only low ester yields can be attained from transesterification. Therefore, the FFA percentage in oil used to produce biodiesel should not exceed 1 wt% before the base-catalyzed transesterification process [18,19]. Regarding biodiesel production from high FFA-containing raw materials, Nakpong et al. (2010) used coconut oil containing 12 wt% FFA to produce biodiesel by a two-step process employing a magnetic stirrer. The FFA content in coconut oil was reduced to less than 0.6 wt% using acid-catalyzed esterification as the first step. The glycerides in the product from the first step were subsequently converted to methyl esters using an alkaline catalyst. The methyl esters (98.4 wt%) were obtained using the following optimal conditions: 0.4 vol% methanol-to-oil ratio, 1.5 wt% catalyst loading, 60 °C reaction temperature, and 60 min reaction time. The properties of the final product showed that the coconut biodiesel met the commercial biodiesel specifications of Thailand [20]. Ghadge et al. (2004) studied biodiesel production from mahua oil (*Madhuca indica*) by a two-step biodiesel process with a 500 mL glass flask and a mechanical stirrer. The high FFA content in mahua oil (19 wt %) was reduced to less than 1 wt% within 60 min at 60 °C with a methanol-to-oil ratio of 0.3–0.35 vol% and sulfuric acid (1 vol%). Transesterification was conducted next with methanol (0.25 vol%) and potassium hydroxide (KOH, 0.7 wt%), which gave a high yield of 98 wt % biodiesel [21]. Their results showed that the fuel properties of mahua biodiesel met the commercial biodiesel standards of the United States and Europe. Velijkovic et al. (2006) studied the production of fatty acid methyl esters (FAMEs) from crude tobacco (*Nicotiana tabacum L.*) seed oil containing 35 wt% of FFA. They employed a two-step reaction process: esterification followed by transesterification. When the molar ratio of methanol to oil was 18:1 and 2 wt% acid catalyst was used, the first step reduced the FFA percentage from 35 to 2 wt% within 25 min. The second step used KOH as the base catalyst and the molar ratio of methanol to triglyceride (TG) was 6:1, where a maximum FAME yield of 91 wt% was obtained in 30 min [22]. Berchmans et al. (2007) investigated biodiesel production from crude Jatropha curacas seed oil (CJCO), where 15 wt% FFA in oil was produced using a 15 cm^3 glass reaction tube with a magnetic stirrer. They found that the FFA content in CJCO decreased from 15 wt% to less than 1 wt% when the first-step was conducted with 1 wt% sulfuric acid and a 0.6 wt% methanol-to-oil mixture over 60 min at 50 °C. The following transesterification process proceeded using a 0.24 wt% methanol-to-oil mixture and 1.4 wt% sodium hydroxide (NaOH), which produced methyl esters in a 90 wt% yield after reacting for 120 min at 65 °C [23].

Various techniques can implement intense mass transfer between immiscible liquids, including mechanical stirrers, static mixers, and microwaves, as well as processes like ultrasonic and hydrodynamic cavitation [24]. Many chemical, food, pharmaceutical, and cosmetic industrial applications have employed static mixers [25], which are particularly suitable for mixing immiscible substances within a short residence time. They are also inexpensive, are easily installed, and require low pumping power [26]. Sungwornpatansakul et al. (2013) compared biodiesel production rates achieved when using a static mixer or a mechanical stirrer. They installed a helical static mixer in a tube with a length of 26 cm and an internal diameter of 0.8 cm and conducted their experiments with a 4.3:1 M ratio of methanol to oil and KOH loadings of 0.6, 1.2, and 1.8 wt%. They concluded that the static mixer employed a larger reaction rate than the mechanical stirrer did. Furthermore, the transesterification reaction was complete within a few seconds when a static mixer was used, whereas mechanical stirring required 30 min to complete the reaction [27].

Chemical reaction rates have also been accelerated using acoustic and hydrodynamic cavitation, which are techniques that have been widely used in biomedical, cleaning, food and beverage, and chemical engineering applications. Acoustic cavitation uses the pressure vibration from an ultrasonic source to create a high frequency in the range of 20 to 100 kHz that is then emitted into a reaction mixture [28]. This ultrasonic cavitation has been commonly used for laboratory-scale biodiesel production. However, this method requires intensive energy consumption, which makes industrial scales quite difficult. It also has a high implementation cost and the ultrasonic cavitation can only be produced near the ultrasonic transducer or horn. [29]. In this study, a rotor–stator reactor was used to induce hydrodynamic cavitation, which can also be called cavitation under a rotary machine. The rotating part of the high-speed rotor was installed in the fixed part of the stator, and the main features of these rotor–stator devices are their high speed and high shear [30]. The rotor and stator develop mixing energy, shear, turbulence, and cavitation. Cavitation generally occurs in liquids maintained at a constant temperature by decreasing the local pressure to a value lower than the vapor pressure. When the local pressure is lower than the vapor pressure, the liquid vaporizes and forms vapor bubbles. Then, the vapor bubbles collapse into the liquid state. As a result, high velocities, pressures, and temperatures can be used, which is greatly important for our system to operate with high efficiency [30]. Similar reports were described by Kim et al. (2020) who investigated sludge disintegration using a rotor–stator hydrodynamic cavitation reactor [31]. They reported that the intensity and area of the cavitation region increased along the rotational direction, and the portion of vapor bubbles quickly collapsed due to pressure recovery and strong shear stress. Moreover, these rotor–stator reactors are very suitable for industrial applications owing to their wide range of cavitation regions, inexpensive equipment, and easy scalability [32].

For cavitation in continuous flow reactors, an orifice plate, Venturi tube, throttling valve, and rotor–stator device were applied to create the cavitation bubble collapse as the mixtures flowed through the cavitation reactors [33]. Moreover, hydrodynamic cavitation can be performed at a reasonable cost and it consumes less energy, has shorter reaction times, and can be applied in large-scale wastewater treatment and biological applications, such as cell disruption and food processing [34]. Ji et al. (2006) analyzed the transesterification process of soybean biodiesel using a mechanical stirrer operating at 900 rpm, an ultrasonic cavitation reactor with a 19.7 kHz frequency, and a hydrodynamic cavitation reactor with a single orifice plate operating at 0.7 MPa. They compared the energy consumption of the mechanical stirrer and two reactors under the same reaction conditions: a molar ratio of 6:1, 1 wt% KOH, and a reaction temperature of 45 °C. They found that the mechanical stirrer consumed 500 W per 1 kg of soybean biodiesel, while the ultrasonic and hydrodynamic reactors consumed 250 W and 183 W, respectively. This suggests that acoustic cavitation and hydrodynamic cavitation reduced energy consumption by 50% and 36.6%, respectively, from that consumed by the mechanical stirrers [35]. Orifice plate- and Venturi-type reactors have been commonly used in biodiesel production and water treatment; however, their major drawback is a high pressure drop in these pipes. The novel rotor–stator technology can be using in emulsification, homogenization, dissolution, dispersion, and grinding processes, as well as chemical reactions and cell disruption, due to their high shear stress, elongational stress, turbulence, cavitation, and energy mixing [30]. A rotor with many holes in its surface is operated inside the reactor, and the high-speed working liquid runs the gap between the rotor and stator [36]. A high-velocity liquid flows through the hollow cavities and a low-pressure region is created near the surface when it exits the system [36].

The present study aimed to optimize continuous esterification for reducing FFA content in mixed CPO (MCPO) using a 3D-printed rotor–stator device in a hydrodynamic cavitation reactor or a hydrosonic reactor. The cost-effective 3D-printed rotor is the essential part of this study. In addition, response surface methodology (RSM) was applied to optimize the amount of methanol and sulfuric acid, the

diameter and depth of the holes, and the speed of the rotor. The yield percentages of each product after reaction and purification, as well as the electricity consumed by the entire biodiesel production process, were also determined.

2. Materials and methods

2.1. Materials

MCPO was obtained from a palm oil extraction factory in southern Thailand, where a single-screw press was used to extract the oil from the palm fruit [37], as shown in Fig. 1. This was used as a feedstock for removing FFAs using a 3D-printed rotor–stator device in a hydrodynamic cavitation reactor. The MCPO consisted of 11.456 wt% FFA, 77.881 wt% TG, 10.353 wt% diglyceride (DG), and 0.309 wt% monoglyceride (MG). Commercial grade methanol (99.7%) and sulfuric acid (99%), as an acid catalyst, were used in the esterification process. Thin-layer chromatography with flame ionization detection (TLC/FID; model: IATROSCAN MK-65, Mishubishi Kagahu Latron Inc., Tokyo, Japan) was used to analyze the esterified oil composition [38]. Analytical-grade hexane, formic acid, diethyl ether, and benzene were used to analyze the MCPO and esterified oil compositions, which consisted of esters, FFAs, TGs, DGs, and MGs.

2.2. Procedure

2.2.1. Experimental setup

The acid-catalyzed esterification of the MCPO was conducted using a hydrosonic reactor that was installed according to the experimental schematic diagram shown in Fig. 2. This reactor was the main component for the continuous esterification process that reduced the FFA content. An acrylonitrile–butadienestyrene (ABS)-filament rotor with a fixed inner diameter of 60 mm and a length of 46 mm was used as the mixing element. The stator was fabricated using stainless steel (SUS304) and was a stationary part of the rotary system. The stator had inner and outer diameters of 80 and 90 mm, respectively. The gap between the rotor and stator (G) was also fixed at 10 mm. Holes were created in the rotor surface where their centers were set at 22.5° angles from one another originating from the center line of the rotor. Therefore, there were 80 spherical holes total, as shown in Fig. 3. The diameter and depth of the holes were varied according to the design of experiments (DOE). The real prototype of the hydrosonic reactor and dimensions of the 3D-printed rotor are described in Fig. 3. The 3D-printed rotor of the

Fig. 1. Production steps of biodiesel using hydrodynamic cavitation (A) mixed crude palm oil, (B) esterified oil (top layer) and generated wastewater (bottom layer), and (C) purified esterified oil after purification.

hydrosonic reactor was driven by a motor (Grundfos, model: MG112MC) via a mechanical shaft. The motor was controlled by adjusting the shaft speed with a variable frequency inverter (Emerson, model: M201). Flexible coupling was used to transmit torque from the mechanical shaft of the motor to the shaft of the rotor, and to support any misalignment between the two shafts. To prevent the reactor from leaking, two flanges with four bolts were assembled to enclose the reactor. When the rotation speed increased, the resultant high rotor speed increased the surface velocity of the liquid on the rotor surface. Consequently, this high-velocity liquid enters the holes and a low-pressure region is formed near the rim of the holes when the liquid exits. This causes cavitation because the surface velocity of the liquid is so high that the pressure near the surface drops to a value lower than or equal to the liquid–vapor pressure [36]. Generally, the MCPO (25 L/h fixed flow rate), methanol, and sulfuric acid were continuously fed into the hydrosonic reactor that housed the inlet valve. Three digital dosing pumps then moved predetermined ratios of these reagents through the rotating rotor in the stator reactor, as detailed in the experimental procedure section. The MCPO flow rate was calibrated for each set of experimental conditions using a graduated cylinder and stopwatch.

2.2.2. 3D printing the hydrosonic reactor rotor

The rotor was printed with a high-performance 3D printer (model: Flashforge Creator3) using ABS filament. Flashprint software version 4.5.1 was installed and setup to obtain the highest quality of the printed product. The average printing time of the rotor was approximately 10 to 11 h, depending on the dimensions of the holes on the surface. All the rotors were created using a high-performance option that employed 100% filling filament and 0.05 mm layer resolution. The layer thickness of the filling filament was set to 0.0025 mm. A hexagonal pattern for the printed rotor infill was used as it is a stronger model for the filling filament (Fig. 3B). Fig. 3D shows the cross-sectional view of the hard surface texture. Using 100% filling filament ensures that the ABS filament will be added until the desired density of the rotor is achieved. If 50% filling filament is used, many hexagonal holes will form inside the rotor (Fig. 3E). As a result, the rotor durability would be reduced, increasing the chance of the mixture in the reactor leaking into the printed model. Therefore, 100% filling filament is recommended for building a prototype rotor for a chemical process. The printed rotor appeared to have a smooth surface (Fig. 3C). Corrosion of the rotor surface after each experimental condition was monitored by visualization and changes in the rotor weight. For all conditions used, there was no change in the rotor weight. The average surface roughness of the 3D-printed rotors was 0.00321 mm, which was determined using a confocal laser scanning microscopy (CLSM). The CLSM is an analyzer to measure the surface topography combined with a high resolution optical imaging with depth selectivity. Since ABS filament was used for printing, its standard melting temperature of 230 °C [39] was the temperature of the nozzle that was used while the 3D printer was operating. Moreover, ABS filament can resist numerous chemicals, such as aqueous acids, alkalis, phosphoric acids, alcohols, animal fats, vegetable oils, and mineral oils [40]. Lopes et al. (2019) studied the manufacturing of 3D-printed, micro-chemical plants for the production of biodiesel using ABS filament and a Sethi3D S3 printer (Campinas, SP, Brazil). They conducted transesterification with NaOH as the base catalyst. The reaction was carried out using an ethanol solution with 0.85 wt% NaOH, an ethanol-to-oil ratio of 14:1, and a temperature of 50 °C. Ethanol and sunflower oil were pumped at 140 and 160 mL/min, respectively. The biodiesel yield from the micro-chemical plants was determined using four milli-reactors, where yields of 51.2 vol%, 43.2 vol%, 31.3 vol%, and 52.3 vol% were achieved for reactor units 1, 2, 3, and 4, respectively [41]. A preliminary study was conducted to test the ABS filament corrosion by monitoring changes in the rotor weight and by visually analyzing the rotor surface. The segment of the filament was soaked in methanol and sulfuric acid for over six months, after which we observed no changes in the rotor weight nor the smoothness of the filament surface. Moreover,
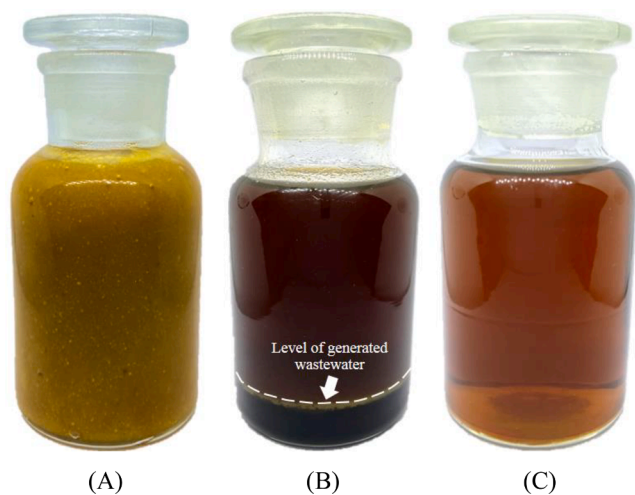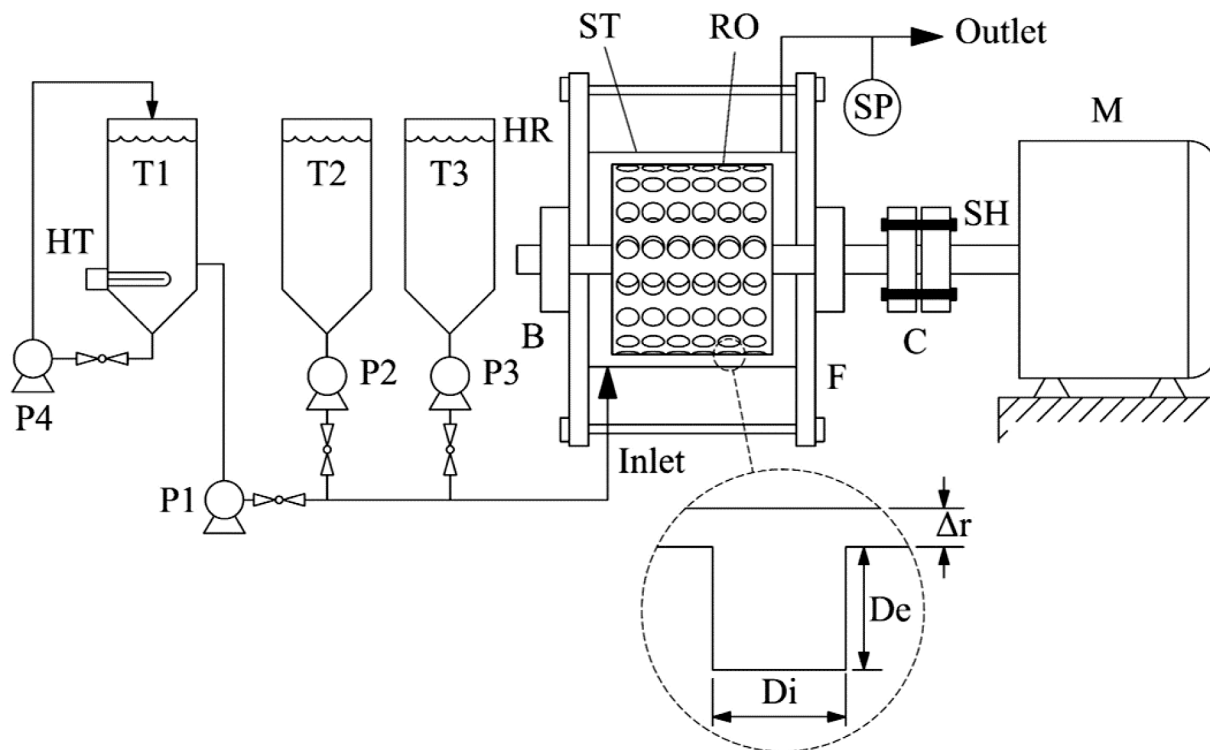
Fig. 2. Schematic diagram for hydrodynamic cavitation experimental setup. (T1: MCPO tank, T2: methanol tank, T3: sulfuric acid tank, P1: MCPO pump, P2: methanol pump, P3: sulfuric acid pump, P4: circulating pump, M: motor, SP: sampling port, HR: hydrosonic reactor, SH: mechanical shaft, C: flexible shaft coupling, F: flange, RO: 3D-printed rotor, ST: stator, D_e: depth of hole, D_i: diameter of hole, B: high speed bearing, and Δr: gap distance between the rotor and stator.

the weight of all the printed rotors was measured after the experimental process to monitor their corrosion. This is because corrosion from the cavitation effect of the chemical reactants may occur at the rotating part of the rotor during the continuous biodiesel production process. Methanol in particular exhibited a high vaporizing effect in the mixtures; therefore, its cavitation effect could corrode the rotor surface. Furthermore, the 3D-printed rotor was tested in triplicate for its use the esterification process where it operated at its highest speed of 5000 rpm to ensure corrosion. After this preliminary study on the corrosion behavior of the ABS rotor, the weight of the 3D-printed rotor was measured using a digital weight balance. The weight of the 3D-printed rotor did not change and the surface of the rotor appeared to be smooth. As the rotation speed of the rotor increases, the cavitation number (CN) decreases [42]. Inception generally occurs at a CN of 1.0, and there are significant cavitation effects at CNs less than 1 [43]). The CN is a dimensionless number used to relate flow conditions to cavitation intensity. For this study, it was calculated based on methanol because methanol has the highest vaporization among the reagents used, and it can be expressed by Eq. (1) [44].

$$CN = \frac{P_2 - P_v}{\frac{1}{2}\rho v^2} \tag{1}$$

Here, P_2 is the downstream pressure at the outlet of the reactor, P_v is the vapor pressure of the flowing liquid, ρ is the density of flowing liquid, and v is the surface velocity of the liquid on the surface of the rotor. For the optimal conditions, the CN was calculated to be 0.5 using Eq. (1), where $P_2 = 101325$ Pa, $P_{v,\text{methanol}} = 84403.4$ Pa at 60 °C, $\rho_{\text{methanol}} = 755$ kg/m^3 at 60 °C, and $v = 9.42$ m/s at 3000 rpm. In addition, when $n = 3000$ rpm (under the optimal conditions) $v = r\omega$, which was calculated to be 9.42 m/s when $\omega = 2\pi n = 2\pi(3000/60) = 314$ rad/s and r = 0.06/2 = 0.03 m.

2.2.3. Experimental procedure

An electric heater was assembled inside tank T1 to preheat the MCPO

to 60 °C to decrease its viscosity. The temperature of the MCPO tank was measured using an electrical thermocouple. A circulating pump (P4, SANSO, model: PMD-37 1) was also used to ensure a stable temperature in T1. When the temperature reached 60 °C, MCPO was pumped continuously into the hydrosonic reactor using a digital dosing pump (P1, Grundfos alldos, model: DME 48-3). At the same time, methanol from T2 and sulfuric acid from T3 were immediately fed into the hydrosonic reactor using chemical resistant pumps P2 (Grundfos alldos, model: DDC 15-4) and P3 (Grundfos alldos, model: DME 2-18), respectively. The motor was then turned on to drive the shaft, which was connected the 3D-printed rotor, to mix the MCPO, methanol, and sulfuric acid. All digital pumps were immediately turned off when the reactant mixture flowed out from the outlet valve of the reactor. The rotor was then rotated in the stator of the hydrosonic reactor, which was operated in batch mode for one residence time (about 20 s) to obtain the equilibrium reaction before the feed pumps were restarted. Three 30 mL samples were taken at 20 s intervals at the outlet valve of the hydrosonic reactor. Every sample from the outlet port was kept in 30 mL glass bottles and immediately cooled to 0 °C with a water bath to stop the reaction. The esterified oil was purified with warm water to remove the generated wastewater and other contaminants. The purified esterified oil comprised esters, FFAs, MGs, DGs, and TGs that were included in its weight percentage, which were investigated using TLC/FID. The optimum conditions were determined by response surface methodology (RSM).

2.3. Experimental design

RSM was applied to optimize the reduction of FFA content from the esterification process using a hydrosonic reactor. Using multiple regression analysis, a second-order polynomial equation was used to obtain the predicted FFA model of the pretreated oil after the esterification process. A general second-order polynomial equation is expressed in Eq. (2).
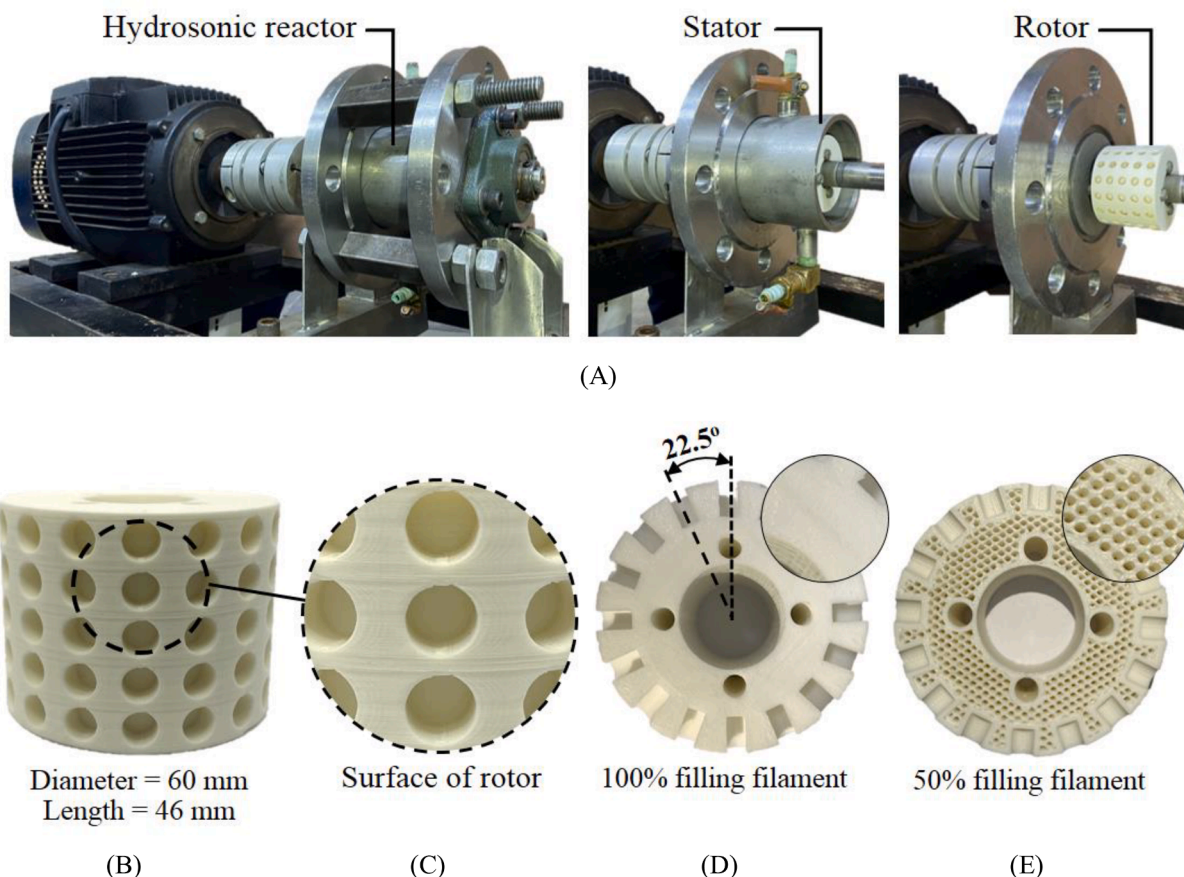
Fig. 3. The real 3D printed rotor–stator hydrodynamic cavitation, (A) real prototype of hydrosonic reactor, (B) dimensions of 3D printed rotor, (C) surface of rotor, (D) 100% filling filament, and (E) 50% filling filament of rotor.

$$Y = \beta_0 + \sum_{i=1}^{k} \beta_i x_i + \sum_{i=1}^{k} \beta_{ii} x_i^2 + \sum_{i=1}^{k} \sum_{j=i+1}^{k} \beta_{ij} x_i x_j + \varepsilon \quad (2)$$

where Y is the response, x_i and x_j are the uncoded independents, β_0 is the constant term, β_i is the coefficient of the linear parameter, β_{ii} is the coefficient of the quadratic parameter, β_{ij} is the coefficient of interaction parameters, k is the number of variables, and ε is the error.

For the reduction of FFA content in MCPO, Y was that of the FFAs (wt %) and the five independent variables were the following: methanol (10–32.5 vol%), sulfuric acid (0.5–4.5 vol%), rotor speed (1000–5000 rpm), hole diameter (3–7 mm), and hole depth (4–10 mm). These five variables were studied to verify the optimal conditions for reducing FFA content from the MCPO using a hydrosonic reactor. The axial parameter (α_x) was equal to 2 (for rotatable central composite designs (CCDs)) when five independent variables were used. Therefore, the coded independent variables were −2, −1, 0, +1, and +2. Table 1 shows the coding system of the independent variables used in this study.

Table 1

Translation table for factor levels in the experimental design for response surface methodology.

Independent variable		Coded level				
		−2	−1	0	+1	+2
M	Methanol (vol%)	2.5	10	17.5	25	32.5
C	Sulfuric acid (vol%)	0.5	1.5	2.5	3.5	4.5
D_i	Diameter of hole (mm)	3	4	5	6	7
D_e	Depth of hole (mm)	2	4	6	8	10
S	Speed of rotor (rpm)	1000	2000	3000	4000	5000

3. Results and discussion

3.1. Experimental results

In this study, 30 experimental conditions using various amounts of methanol and sulfuric acid, different hole diameters and depths, and various rotor speeds were designed and tested using the DOE. The results from reducing the amount of FFAs via esterification with a hydrosonic reactor are listed in Table 2. To successfully convert the MCPO to highly pure biodiesel through this two-step process, less than 1 wt% FFA should be present in the pretreated oil. Therefore, it is crucial to reduce the FFA content before the glycerides are converted to esters in the pretreated oil.

3.2. Response surface methodology and statistical analyses

RSM was used to reduce FFA content during a continuous esterification process with a hydrosonic reactor and model fitting by multiple regression. The predictive models in Eq. (3) are multivariate second-order polynomials. The coefficients of the respective fitted models, p-values for the individual terms, coefficient of determination (R^2), and the adjusted coefficient of determination ($R^2_{adjusted}$) are shown in Table 3. The analysis of variance (ANOVA) for each RSM term representing the continuous esterification process is listed in Table 4.

$$\text{FFA} = \beta_0 + \beta_1 D_i + \beta_2 D_e + \beta_3 M + \beta_4 C + \beta_5 D_i^2 + \beta_6 D_i M + \beta_7 D_e^2 + \beta_8 D_e S + \beta_9 SM + \beta_{10} C^2$$

$$(3)$$

Here, the following variables represent the independent variables of this

Table 2
Design of experiments of continuous esterification process FFA reduction.

Run	M (vol%)	C (vol%)	D_i (mm)	D_e (mm)	S (rpm)	FFA (wt%)
1	17.5	2.5	5	6	3000	2.199
2	17.5	2.5	5	6	3000	2.118
3	17.5	2.5	5	6	3000	2.130
4	17.5	2.5	5	6	3000	2.162
5	2.5	2.5	5	6	3000	2.895
6	17.5	0.5	5	6	3000	0.656
7	17.5	4.5	5	6	3000	0.176
8	17.5	2.5	5	6	1000	2.461
9	17.5	2.5	5	6	5000	1.718
10	32.5	2.5	5	6	3000	1.419
11	17.5	2.5	5	2	3000	0.129
12	17.5	2.5	5	10	3000	0.235
13	25.0	1.5	4	4	2000	0.704
14	10.0	1.5	4	4	4000	0.573
15	10.0	3.5	4	4	2000	0.015
16	25.0	3.5	4	4	4000	0.027
17	25.0	3.5	4	8	2000	0.053
18	10.0	1.5	4	8	2000	0.029
19	10.0	3.5	4	8	4000	0.853
20	25.0	1.5	4	8	4000	0.740
21	25.0	3.5	6	4	2000	0.692
22	10.0	1.5	6	4	2000	1.536
23	10.0	3.5	6	4	4000	2.118
24	25.0	1.5	6	4	4000	0.311
25	10.0	3.5	6	8	2000	0.855
26	25.0	3.5	6	8	4000	0.260
27	10.0	1.5	6	8	4000	2.639
28	25.0	1.5	6	8	2000	0.049
29	17.5	2.5	3	6	3000	0.008
30	17.5	2.5	7	6	3000	1.062

Note: D_i is diameter of hole, D_e is depth of hole, M is methanol, C is sulfuric acid, S is speed of rotor, FFA is free fatty acid, and 25 L/hr of MCPO flow rate was fixed in all experiments.

Table 3
Coefficients in the fitted response surface model.

Coefficient	Value	p-value
β_0	−20.29	0.000000000119
β_1	5.328	0.000000003521
β_2	1.179	0.000000722215
β_3	0.294	0.000008726700
β_4	2.114	0.000000085774
β_5	−0.415	0.000000079413
β_6	−0.0491	0.000019716100
β_7	−0.126	0.000000003862
β_8	0.00011	0.000048254834
β_9	0.000032	0.000183695684
β_{10}	−0.445	0.000000027510

Note: The coefficient of determination (R^2) is 0.974, and the adjusted coefficient of determination ($R^2_{adjusted}$) is 0.949.

Table 4
ANOVA for each response surface model representing the continuous process.

Source	SS	MS	F_0	F_{crit}	DOF
Regression	23.93	2.393	35.02	2.3779 ($F_{0.05,10,19}$)	10
Residual (Error)	1.298	0.06832			19
Lack-of-Fit Error	1.294	0.08088			16
Pure Error	0.00393	0.00131			3
Total	25.22				29

Note: DOF is degrees of freedom, SS is sum of squares, and MS is mean square.

process: M represents methanol (vol%), C is sulfuric acid (vol%), D_i is the diameter of hole (mm), D_e is the depth of the hole (mm), S is the speed of the rotor (rpm), and β is a fixed coefficient.

The statistical significance of every regression coefficient in the models depends on their *p*-values. If the *p*-values are less than 0.05 at the 95% confidence level, the results will be statistically significant. A detailed list of each parameter is described in Table 3. Lower *p*-values were found for terms $\beta_1 D_i$ and $\beta_7 D_e^2$. Therefore, the D_i and D_e were influenced by the terms $\beta_1 D_i$ and $\beta_7 D_e^2$, respectively, and had almost similar levels of significance. Furthermore, the D_i and D_e greatly impacted the reduction of FFAs present in the MCPO. The smallest *p*-values are the most essential for reducing the FFA level with a continuous esterification process using a hydrosonic reactor. The quadratic term of the acid catalyst ($\beta_{10}C^2$) was ranked third. ANOVA was used to determine the significance of the predictive models, as shown in Table 4. When using the *F*-test to determine model significance, the *F*-test statistic (F_0) value must be greater than the critical value (F_{crit}). The critical value is regarded as $F_{\alpha, n-1-i}$, where α is the axial point for rotability, n is the number of experiments, and *i* is the number of coefficients. Using the *F*-distribution table to obtain a critical value at 95% confidence (Table 4), F_0 was found to be greater than F_{crit}. Therefore, the predictive model was statistically significant for FFA-content reduction.

3.3. Response surface plots

Fig. 4 shows a contour plot illustration of the FFA-content reduction according to the relationships between the dependent variable (FFA wt %) and independent variables (methanol, sulfuric acid, D_i, D_e, and S) of the continuous esterification process.

3.4. Optimal conditions for reducing FFA content in the MCPO

The optimal conditions for removing FFAs during MCPO esterification were determined by applying the model in Eq. (3). The weight percentage of FFA in oil should not exceed 1 wt% before the base-catalyzed transesterification process is conducted to produce biodiesel. Consequently, 1 wt% FFA was inserted into Eq. (3) to give the dependent variable FFA. The independent variables M, C, D_i, D_e, and S were solved using the Microsoft Excel solver tool. The results showed that 1 wt% FFA was achieved at the optimal conditions of 17.7 vol% methanol, 2.9 vol% sulfuric acid, a D_i of 4 mm, a D_e of 6 mm, and an S of 3000 rpm.

3.5. Effect of the hole dimensions on the rotor surface

According to the statistical analysis of the RSM, the most significant parameters in this study for lowering the FFA level were D_i and D_e. The effect of these parameters on the FFA-reduction contour plot is shown in Fig. 4C. When the D_e was less than 4 mm or greater than 6.5 mm and the D_i was less than 4 mm or greater than 8 mm, 1 wt% FFA was found in the holes. A higher value of FFA (2 wt%) was achieved when the D_e was in the range of 4.5 to 6.0 mm and the D_i was between 5 and 7 mm. The RSM was employed to study the effect of various hole dimensions on the rotor surface for FFA-content reduction. The conditions of cavitation and efficiency depend on the operating parameters (e.g., changing inlet pressure) and the size and shape of the holes. Furthermore, the intensity of collapsing cavities depends on the configuration of the cavitation device under various flow conditions [45]. Kim et al. (2020) reported the use of rotor–stator hydrodynamic cavitation for sludge disintegration. They studied the effects of particle size distribution, cavitation, and shear stress on the sludge disintegration process when the hydrodynamic reactor was operated with and without dimples. As a result, most sludge particles were 10–100 μm in size when dimples were not used but were 1–10 μm in size when dimples were used. The particle decomposition performance depended on cavitation, which is due to shear stress. They reported that when dimples were not used particle decomposition did not change even when the shear stress was increased [31].

In addition, continuous biodiesel production from waste cooking oil (WCO) using a shockwave power reactor was evaluated by Abbaszadeh-mayvan et al. (2018). They analyzed five operating parameters, such as the ratio of cavity depth to the gap between rotor and stator, the ratio of rotor diameter to stator diameter (D_r/D_s), rotor speed, and residence time. They reported that the D_r/D_s was the most essential parameter
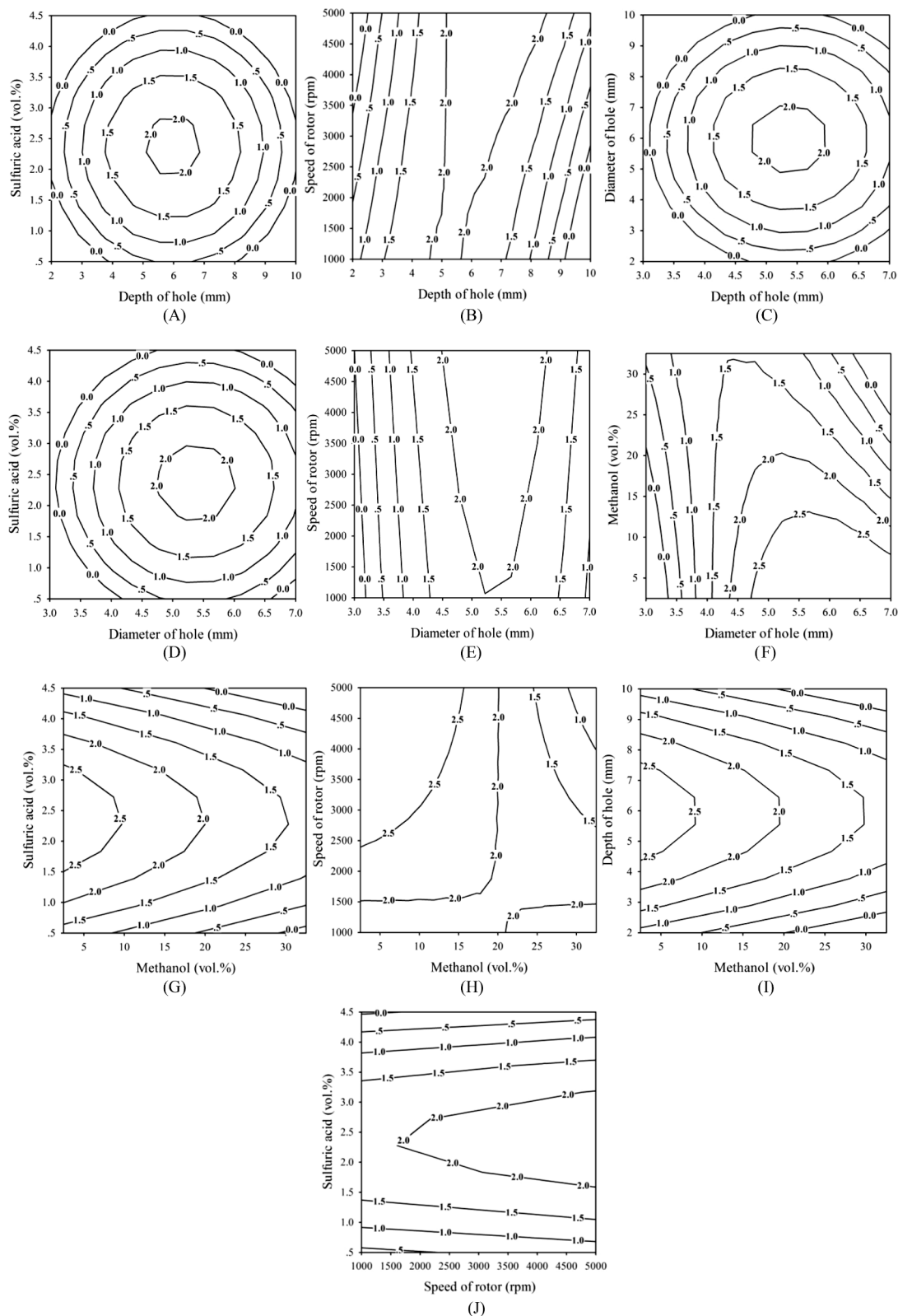
Fig. 4. Contour plots of optimized condition for continuous process (A, B and C) effects of depth of hole and H_2SO_4, speed of rotor and diameter of hole; (D, E and F) effects of diameter of hole and H_2SO_4, speed of rotor and MeOH; (G, H and I) effects of MeOH and H_2SO_4, speed of rotor and depth of hole; (J) effects of speed of rotor and H_2SO_4 on the reduction of free fatty acid.

effecting the yield of FAMEs, which aligns well with the results of this study. In this study, D_e and D_i were the most important parameters for FFA-content reduction. Regarding orifice and Venturi cavitation devices, the condition of cavitation inside a cavitation device can be changed by varying the ratio of the throat length to the diameter/height, the divergence angle, and the ratio of the cavitation hole perimeter to the cross-sectional area [46]. Most studies used single or multi-hole orifice plates to create a cavitation bubble in the pipeline. Research related to the effect of the geometry of multi-hole orifices on the degradation of a rhodamine B (RhB) solution (a cationic dye) has been studied by Sivakumar and Pandit (2002) [47]. They stated that the cavitational production was improved by varying the flow geometry and pressure fluctuations of a turbulent pressure [47]. A numerical simulation was analyzed to optimize the essential geometric parameters of the cavitating venturi using computational fluid dynamics (CFD). They reported that the capacity of a cavitating device to generate cavities and the overall cavitational yield relied on the ratio of the hole perimeter to the cross-sectional flow area, the ratio of the throat length to height, and the divergence angle. A few studies have reported optimized geometries and shapes of different cavitating devices using actual experiments [48].

3.6. Verification, yield, and residual methanol

The amount of FFAs reduced via the esterification process using optimal conditions was verified by TLC/FID. The actual experiment gave oil with a reduce amount (1.028 wt%) of FFA at a 25 L/h MCPO flow rate, as shown in Table 5. The FFA content in the preheated oil was very close to the 1 wt% that was theoretically predicted. The yield of crude biodiesel was 96.07 vol%, which was calculated based on 100 vol% of the initial MCPO being obtained under the optimal conditions. Fig. 1B shows the esterified oil after the complete phase separation process, where gravity separation took at least 6 h to separate the black phase of the generated wastewater, which settled to the bottom of the sampling bottle. Before the purification process, the obtained esterified oil contained residual methanol and generated wastewater. The amount of purified esterified oil was calculated to determine the average purified esterified oil yield by volume per liter of MCPO. The results showed that the continuous esterification process gave the purified esterified oil in 91.27 vol% yield (Fig. 1C) after washing (calculated based on the 100 vol% of MCPO). Excess methanol was used for the esterification reaction to achieve good FFA conversion. Furthermore, the esterified oil and generated wastewater were tested using gas chromatography (GC) [49]. The results indicated 8.305 vol% of residual methanol remained in the generated wastewater. Therefore, one concern is recovering this residual methanol for reuse in the first step of esterification. A methanol-recovery unit should be used in pilot and industrial-scale biodiesel production from FFA-rich oils. The residual methanol content in the esterified oil was 1.383 vol%, which could easily be used in the next step for producing biodiesel.

3.7. Electricity consumption for continuous esterification process

A digital power meter was used to measure the average electricity consumed by the entire process (Table 6). The startup preparation for preheating MCPO to 60 °C included installing an immersion heater and circulating pump that used 0.56 kW to provide the 25 L MCPO tank with a stable temperature. The electrical motor consumed 0.569 kW h to drive the rotor inside the hydrosonic reactor. Three digital dosing pumps used a total of 0.034 kW h to feed MCPO, methanol, and sulfuric acid into the reactor. The rotor–stator hydrodynamic cavitation reactor consumed 0.603 kW h to produce 22.8 L of purified biodiesel from 25 L of MCPO. Therefore, the average electrical energy consumed to produce crude biodiesel was 0.0264 kW h/L.

4. Conclusions

In this work, a novel 3D-printed rotor–stator hydrodynamic cavitation reactor was effectively applied to reduce the amount of FFAs present in MCPO using a continuous esterification process. The optimal conditions to reduce FFA content to 1 wt% were predicted using RSM and were as follows: 17.7 vol% methanol, 2.9 vol% sulfuric acid, a D_i of 4 mm, a D_e of 6 mm, and a rotor speed of 3000 rpm. The FFA content in the MCPO was reduced to 1.028 wt% when these optimal conditions were used. Esterified oil was obtained in a maximum yield of 96.07 vol% from the phase separation step, and 91.27 vol% purified oil was isolated after purification. An average electricity consumption of 0.0264 kW h/L was measured for the entire esterification process using a 3D-printed rotor–stator device in a hydrodynamic cavitation reactor. This study demonstrated that 3D-printed, rotor–stator cavitational reactors could be efficiently applied to reduce FFA content, which is a key step for efficient biodiesel production. However, this printed rotor was mainly considered for the esterification reaction because it is cost effective and requires little time to construct; therefore, its application could effectively reduce manufacturing costs. Such a 3D-printed rotor was used for a preliminary study to determine the optimal operating conditions. For practical industrial processes, long-living, stainless steel rotors with numerous holes on their surface are manufactured by computer numerical control (CNC) machines. This method is applied to obtain precise positioning of the drill hole on the rotor surface. However, employing CNC machines is expensive. Metal 3D printing is a less expensive alternative that uses a laser-based technology and powdered metals for producing rotors. The devices and parts manufactured with metal materials are highly resistant to most chemicals and can be applied in automotive, aerospace, and medical applications [50]. Therefore, many different materials can be used for additive manufacturing or 3D-printing technology. This method could also potentially benefit construction and other industrial fields. However, the prices of metal 3D printing are still relatively high [50]. Thus, it may not be worth acquiring a metal 3D printer to overcome design limitations

Table 5

Physical property, composition, yield, and residual methanol of MCPO and esterified oil.

Composition[a], yield[b], and residual methanol	MCPO	Esterified oil[a]
Free fatty acid (wt%)	11.46	1.028
Methyl ester (wt%)		5.138
Triglyceride (wt%)	77.88	89.67
Diglyceride (wt%)	10.35	4.061
Monoglyceride (wt%)	0.309	0.102
Density		
at 60 °C (kg/L)	0.883	0.889
at 32 °C, room temperature (kg/L)	0.91	0.894
Yield[b]		
Eterified oil (vol%)		96.07
Generated wastewater (vol%)		24.53
Purified esterified oil (vol%)		91.27
Residual methanol		
Residual methanol in esterified oil (vol%)		1.383
Residual methanol in generated wastewater (vol%)		8.305

[a] Result of actual experiment
[b] Yield of esterification process (vol%) = the volume of product (mL)/the volume of initial MCPO (mL). The yields are relative to 100 vol% of initial MCPO.

Table 6

Average electricity consumption in the continous esterification process.

Continous process steps	Electricity (kWh)	
	Start up	Process
25L of MCPO was preheated to 60 °C within 15 min	0.56	
Three electrical dosing pumps: MCPO, MeOH and H_2SO_4		0.034
Running motor for hydrosonic reaction		0.569
Total average electricity	0.56	0.603

and rotor durability when plastic 3D-printing is cheaper and provides effective rotors.

Declaration of Competing Interest

The authors declare that they have no known competing financial interests or personal relationships that could have appeared to influence the work reported in this paper.

Acknowledgement

References

[1] S. Manprasert, Thailand industry outlook 2018–20: Biodiesel, Krungsri Res. (2018).

[2] N.-O. Nylund, P. Aakko-Saksa, K. Sipilä, Status and Outlook For Biofuels, Other Alternative Fuels And New Vehicles, VTT, Espoo, 2008.

[3] A. Kumar, S. Sharma, Potential non-edible oil resources as biodiesel feedstock: An Indian perspective, Renew. Energy Rev. 15 (2011) 1791–1800, https://doi.org/10.1016/j.rser.2010.11.020.

[4] S. Kumar, P. Salam, P. Shrestha, E. Ackom, An assessment of Thailand's biofuel development, Sustainability 5 (2013) 1577–1597, https://doi.org/10.3390/su5041577.

[5] M.J. Iskandar, A. Baharum, F.H. Anuar, R. Othaman, Palm oil industry in South East Asia and the effluent treatment technology—A review, Environ. Technol. Innov. 9 (2018) 169–185, https://doi.org/10.1016/j.eti.2017.11.003.

[6] B. Wicke, R. Sikkema, V. Dornburg, A. Faaij, Exploring land use changes and the role of palm oil production in Indonesia and Malaysia, Land Use Policy. 28 (2011) 193–206, https://doi.org/10.1016/j.landusepol.2010.06.001.

[7] Monthly biodiesel data. Department of Alternative energy development and efficiency, Ministry of energy, Thailand, http://110.164.168.126/ewt_news.php?nid=47882&filename=index/; 2020 [accessed 30 June, 2020].

[8] Sontirat steps up campaign for B10 biodiesel use, (n.d.). https://www.nationthailand.com/news/30380042 (accessed July 22, 2020).

[9] Biodiesel-Krungsri Research. Thailand industry outlook 2020-22, https://www.krungsri.com/bank/getmedia/0b29b5f1-30eb-40d6-a2fb- d04789ab2dd5/IO_Biodiesel_200108_EN_EX.aspx [accessed 28 June, 2020].

[10] WHO | Ambient air pollution: Health impacts, WHO. (n.d.). http://www.who.int/airpollution/ambient/health-impacts/en/ (accessed June 28, 2020).

[11] N. Traviss, Breathing easier? The known impacts of biodiesel on air quality, Biofuels 3 (2012) 285–291, https://doi.org/10.4155/bfs.12.22.

[12] N.S. El-Gendy, S.F. Deriase, Application of statistical approaches to optimize the productivity of biodiesel and investigate the physicochemical properties of the bio/petro-diesel blends, in: High-Performance Materials and Engineered Chemistry, Apple Academic Press, 2018, pp. 161–239.

[13] F.B. Ahmad, Z. Zhang, W.O.S. Doherty, I.M. O'Hara, The outlook of the production of advanced fuels and chemicals from integrated oil palm biomass biorefinery, Renew. Sustain. Energy Rev. 109 (2019) 386–411, https://doi.org/10.1016/j.rser.2019.04.009.

[14] N. Fold, L. Whitfield, Dansk Institut for Internationale Studier, Developing a palm oil sector: the experiences of Malaysia and Ghana compared, Danish Institute for International Studies, Copenhagen, 2012.

[15] S. Kadandale, R. Marten, R. Smith, The palm oil industry and noncommunicable diseases, Bull. World Health Organ. 97 (2019) 118–128, https://doi.org/10.2471/BLT.18.220434.

[16] V. Strezov, T.J. Evans, Biomass Processing Technologies, CRC Press, 2014.

[17] V. Seithtanabutara, C. Sungnat, T. Wongwuttanasatian, Comparison of free fatty acid conversion yields for esterification assisted by single- and dual-frequency sonication, Biomass Conv. Bioref. (2020), https://doi.org/10.1007/s13399-020-00659-4.

[18] A. Hayyan, M.Z. Alam, M.E.S. Mirghani, N.A. Kabbashi, N.I.N.M. Hakimi, Y.M. Siran, S. Tahiruddin, Reduction of high content of free fatty acid in sludge palm oil via acid catalyst for biodiesel production, Fuel Process. Technol. 92 (2011) 920–924, https://doi.org/10.1016/j.fuproc.2010.12.011.

[19] S. Jansri, S.B. Ratanawilai, M.L. Allen, G. Prateepchaikul, Kinetics of methyl ester production from mixed crude palm oil by using acid-alkali catalyst, Fuel Process. Technol. 92 (2011) 1543–1548, https://doi.org/10.1016/j.fuproc.2011.03.017.

[20] P. Nakpong, S. Wootthikanokkhan, High free fatty acid coconut oil as a potential feedstock for biodiesel production in Thailand, Renewable Energy 35 (2010) 1682–1687, https://doi.org/10.1016/j.renene.2009.12.004.

[21] S.V. Ghadge, H. Raheman, Biodiesel production from mahua (Madhuca indica) oil having high free fatty acids, Biomass Bioenergy 28 (2005) 601–605, https://doi.org/10.1016/j.biombioe.2004.11.009.

[22] V. Veljkovic, S. Lakicevic, O. Stamenkovic, Z. Todorovic, M. Lazic, Biodiesel production from tobacco (Nicotiana tabacum L.) seed oil with a high content of free fatty acids, Fuel 85 (2006) 2671–2675, https://doi.org/10.1016/j.fuel.2006.04.015.

[23] H.J. Berchmans, S. Hirata, Biodiesel production from crude Jatropha curcas L. seed oil with a high content of free fatty acids, Bioresour. Technol. 99 (2008) 1716–1721, https://doi.org/10.1016/j.biortech.2007.03.051.

[24] A. Bokhari, L.F. Chuah, S. Yusup, J.J. Klemeš, M.M. Akbar, R.N.M. Kamil, Cleaner production of rubber seed oil methyl ester using a hydrodynamic cavitation: optimisation and parametric study, J. Cleaner Prod. 136 (2016) 31–41, https://doi.org/10.1016/j.jclepro.2016.04.091.

[25] A. Ghanem, T. Lemenand, D. Della Valle, H. Peerhossaini, Static mixers: Mechanisms, applications, and characterization methods – A review, Chem. Eng. Res. Des. 92 (2014) 205–228, https://doi.org/10.1016/j.cherd.2013.07.013.

[26] A. Paglianti, Recent innovations in turbulent mixing with static elements, CHENG 1 (2010) 80–87, https://doi.org/10.2174/1874478810801010080.

[27] P. Sungwornpatansakul, J. Hiroi, Y. Nigahara, T.K. Jayasinghe, K. Yoshikawa, Enhancement of biodiesel production reaction employing the static mixing, Fuel Process. Technol. 116 (2013) 1–8, https://doi.org/10.1016/j.fuproc.2013.04.019.

[28] M. Gallo, L. Ferrara, D. Naviglio, Application of ultrasound in food science and technology: A Perspective, Foods 7 (2018), https://doi.org/10.3390/foods7100164.

[29] M. Ashokkumar, Advantages, disadvantages and challenges of ultrasonic technology, in: Ultrasonic Synthesis Of Functional Materials, Springer International Publishing, Cham, 2016, pp. 41–42, https://doi.org/10.1007/978-3-319-28974-8_3.

[30] V.A. Atiemo-Obeng, R.V. Calabrese, Rotor–stator mixing devices, in: Handbook of industrial mixing, John Wiley & Sons, Ltd, 2004, pp. 479–505, https://doi.org/10.1002/0471451452.ch8.

[31] H. Kim, B. Koo, X. Sun, J.Y. Yoon, Investigation of sludge disintegration using rotor- stator type hydrodynamic cavitation reactor, Sep. Purif. Technol. 240 (2020), 116636, https://doi.org/10.1016/j.seppur.2020.116636.

[32] G. Grillo, L. Boffa, A. Binello, S. Mantegna, G. Cravotto, F. Chemat, T. Dizhbite, L. Lauberte, G. Telysheva, Cocoa bean shell waste valorisation; extraction from lab to pilot-scale cavitational reactors, Food Res. Int. 115 (2019) 200–208, https://doi.org/10.1016/j.foodres.2018.08.057.

[33] V.S. Moholkar, A.B. Pandit, Modeling of hydrodynamic cavitation reactors: a unified approach, Chem. Eng. Sci. 56 (2001) 6295–6302, https://doi.org/10.1016/S0009-2509(01)00253-6.

[34] M. Langone, R. Ferrentino, G. Trombino, W.D. Puiseau, G. Andreottola, E.C. Rada, M. Ragazzi, Application of a novel hydrodynamic cavitation system in wastewater treatment plants, UPB Sci. Bull. Series D 77 (2015) 225–234.

[35] J. Ji, J. Wang, Y. Li, Y. Yu, Z. Xu, Preparation of biodiesel with the help of ultrasonic and hydrodynamic cavitation, Ultrasonics 44 (2006) e411–e414, https://doi.org/10.1016/j.ultras.2006.05.020.

[36] M. Badve, P. Gogate, A. Pandit, L. Csoka, Hydrodynamic cavitation as a novel approach for wastewater treatment in wood finishing industry, Sep. Purif. Technol. 106 (2013) 15–21, https://doi.org/10.1016/j.seppur.2012.12.029.

[37] K. Somnuk, J. Thawornprasert, P. Chanjula, G. Prateepchaikul, Response surface methodology optimization of oil extraction from oil palm meal (OPM) with hydrous ethanol and its pilot-scale application with recirculation of extraction solvent, Aust. J. Crop Sci. 13 (2019) 954–965, https://doi.org/10.21475/ajcs.19.13.06.p1705.

[38] K. Somnuk, P. Smithmaitrie, G. Prateepchaikul, Two-stage continuous process of methyl ester from high free fatty acid mixed crude palm oil using static mixer coupled with high-intensity of ultrasound, Energy Convers. Manage. 75 (2013) 302–310, https://doi.org/10.1016/j.enconman.2013.06.033.

[39] S.R. Gonzalez, D.B. Bennett, 3D Printing: A Practical Guide For Librarians, Rowman & Littlefield, 2016.

[40] Plastics Chemical Resistance Chart | Curbell Plastics, (n.d.). https://www.curbellplastics.com/Research-Solutions/Chemical-Resistance-of-Plastics (accessed June 30, 2020).

[41] M.G.M. Lopes, H.S. Santana, V.F. Andolphato, F.N. Russo, J.L. Silva, O.P. Taranto, 3D printed micro-chemical plant for biodiesel synthesis in millireactors, Energy Convers. Manage. 184 (2019) 475–487, https://doi.org/10.1016/j.enconman.2019.01.090.

[42] V.K. Saharan, D.V. Pinjari, P.R. Gogate, A.B. Pandit, Advanced oxidation technologies for wastewater treatment, in: Industrial Wastewater Treatment, Recycling and Reuse, Elsevier, 2014, pp. 141–191, https://doi.org/10.1016/B978-0-08-099968-5.00003-9.

[43] Y.T. Shah, A.B. Pandit, V.S. Moholkar, Cavitation Reaction Engineering, Springer, US, Boston, MA, 1999 https://doi.org/10.1007/978-1-4615-4787-7.

[44] A. Šarc, T. Stepišnik-Perdih, M. Petkovšek, M. Dular, The issue of cavitation number value in studies of water treatment by hydrodynamic cavitation, Ultrason. Sonochem. 34 (2017) 51–59, https://doi.org/10.1016/j.ultsonch.2016.05.020.

[45] V.K. Saharan, M.A. Rizwani, A.A. Malani, A.B. Pandit, Effect of geometry of hydrodynamically cavitating device on degradation of orange-G, Ultrason. Sonochem. 20 (2013) 345–353, https://doi.org/10.1016/j.ultsonch.2012.08.011.

[46] A. Abbaszadeh-Mayvan, B. Ghobadian, G. Najafi, T. Yusaf, Intensification of continuous biodiesel production from waste cooking oils using shockwave power reactor: process evaluation and optimization through response surface methodology (RSM), Energies. 11 (2018) 2845, https://doi.org/10.3390/en11102845.

[47] M. Sivakumar, A.B. Pandit, Wastewater treatment: a novel energy efficient hydrodynamic cavitational technique, Ultrason. Sonochem. 9 (2002) 123–131, https://doi.org/10.1016/S1350-4177(01)00122-5.

[48] T.A. Bashir, A.G. Soni, A.V. Mahulkar, A.B. Pandit, The CFD driven optimisation of a modified venturi for cavitational activity, Can. J. Chem. Eng. 89 (2011) 1366–1375, https://doi.org/10.1002/cjce.20500.

[49] E. de A.S. Braga, J. de Q. Malveira, M.A.L. Milhome, M.D. de Aquino, R.F. do Nascimento, Characterization of the fatty acids present in wastewaters from production of biodiesel tilapia, J. Chem. 2015 (2015) 1–6, https://doi.org/10.1155/2015/265160.

[50] C. Buchanan, L. Gardner, Metal 3D printing in construction: A review of methods, research, applications, opportunities and challenges, Eng. Struct. 180 (2019) 332–348, https://doi.org/10.1016/j.engstruct.2018.11.045.